Proceedings of the
International Conference on Mechanical Engineering 2009
(ICME2009) 26- 28 December 2009, Dhaka, Bangladesh

ICME09-TH-23

STEADY-STATE SOLUTIONS OF HEAT AND MASS TRANSFER FLOW FROM A VERTICAL POROUS PLATE WITH THERMAL DIFFUSION AND INDUCED MAGNETIC FIELD

M. Mohidul Haque and M. Mahmud Alam

Mathematics Discipline, Khulna University, Khulna, Bangladesh

ABSTRACT

The unsteady MHD heat and mass transfer flow past a moving semi-infinite vertical porous plate with thermal diffusion has been investigated numerically taking into account the induced magnetic field. The steady-state numerical solutions for the velocity field, induced magnetic field, temperature distribution and concentration distribution are obtained by the explicit finite difference method. The local and average shear stress, current density, Nusselt number as well as Sherwood number are also calculated. The obtained results have been shown graphically. Also the stability and convergence of the explicit finite difference scheme are established. Finally, the comparison of the present results with both analytical and numerical solutions is presented in tabular form.

Keywords: MHD, Thermal Diffusion, Induced Magnetic Field, Finite Difference Method.

1. INTRODUCTION

The science of magnetohydrodynamics was concerned with geophysical and astrophysical problems for a number of years. In recent years the possible use of MHD is to affect a flow stream of an electrically conducting fluid for the purpose of thermal protection, braking, propulsion and control. From the point of applications, the effect of magnetic field on free convective flows was analyzed by Raptis and Singh[1]. Singh et al.[2] studied MHD heat and mass transfer flow of a viscous incompressible fluid past an infinite vertical porous plate under oscillatory suction velocity normal to the plate. The steady laminar flow and heat transfer characteristics of a continuously moving vertical sheet of extruded material was investigated by Sami and Al-Sanea[3]. The unsteady MHD heat and mass transfer problem with variable suction velocity have studied by Chamkha[4].

The effect of thermal diffusion on MHD free convection and mass transfer flows have many application in separation processes as isotope separation and mixtures between gases with very light molecular weight (H_2, H_e) and medium molecular weight (N_2 , air) (Eckert and Drake[5]). Transient MHD heat and mass transfer flow with thermal diffusion in a rotating system has analyzed by Alam and Sattar[6]. Recently, Alam et al.[7] have numerically investigated the mass transfer flow past a vertical porous medium with heat generation and thermal diffusion on the combined free-forced convection under the influence of transversely applied magnetic field. The problem becomes more complicated if the strong magnetic field has been considered. These types of problems have special importance in astrophysical and geophysical engineering.

Hence our main aim is to investigate steady-state solutions of unsteady MHD heat and mass transfer flow of an electrically conducting viscous fluid past a moving semi-infinite vertical porous plate under the action of strong magnetic field taking into account the induced magnetic field with thermal diffusion.

2. MATHEMATICAL MODEL OF FLOW

Consider MHD combined heat and mass transfer unsteady flow of an electrically conducting incompressible viscous fluid past an electrically non-conducting continuously moving semi-infinite vertical porous plate with thermal diffusion. The flow is assumed to be in the *x*-direction, which is chosen along the plate in upward direction and *y*-axis is normal to it. A strong uniform magnetic field is applied normal to the flow region. Initially it is assumed that fluid and the plate are at rest after that the plate is moved with a constant velocity U_0 in its own plane. Instantaneously at time $t > 0$, temperature of the plate and species concentration are raised to $T_w (> T_\infty)$ and $C_w (> C_\infty)$ respectively, which are thereafter maintained constant, where T_w , C_w are temperature and species concentration at the wall and T_∞ , C_∞ are temperature and species concentration far away from the plate respectively. The physical model of this study is presented in Fig 1.

In addition, the viscous dissipation and joule heating terms in the energy equation have been

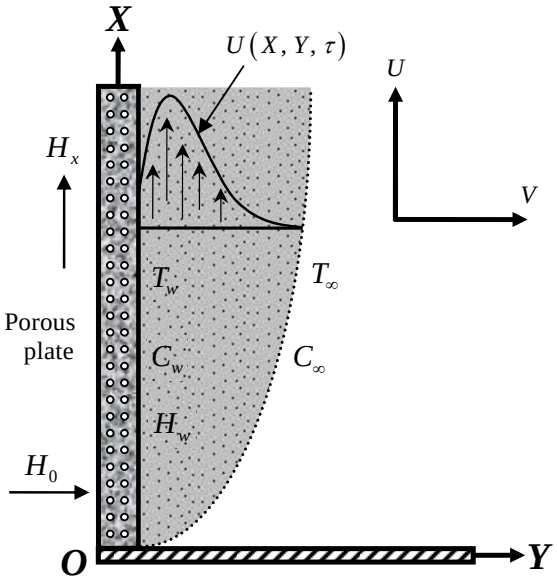

Fig 1. Physical model and coordinate system

considered for high speed flows, the level of concentration of foreign mass has been taken very high for observing the effect of Soret number on flow and the magnetic Reynolds number of flow is taken to be large enough so that the induced magnetic field is not negligible. The divergence equation $\nabla.\mathbf{H}=0$ of Maxwell's equation for the magnetic field gives $H_y =$ constant $= H_0$.

Within the framework of the above stated assumptions and using the dimensionless quantities,

$$X=\frac{xU_0}{\upsilon}\ ,\quad Y=\frac{yU_0}{\upsilon}\ ,\quad U=\frac{u}{U_0}\ ,\quad V=\frac{v}{U_0}\ ,\quad \tau=\frac{tU_0^2}{\upsilon}\ ,$$

$$\bar{H}_x=\sqrt{\frac{\mu_e}{\rho}}\frac{H_x}{U_0}\ ,\ \bar{T}=\frac{T-T_\infty}{T_w-T_\infty}\ \text{and}\ \bar{C}=\frac{C-C_\infty}{C_w-C_\infty}\ ,$$

the equations relevant to the unsteady two dimensional problem is governed by the following non-dimensional system of coupled non-linear partial differential equations under the boundary-layer approximations as;

$$\frac{\partial U}{\partial X}+\frac{\partial V}{\partial Y}=0 \tag{1}$$

$$\frac{\partial U}{\partial \tau}+U\frac{\partial U}{\partial X}+V\frac{\partial U}{\partial Y}=G_r\bar{T}+G_m\bar{C}+\frac{\partial^2 U}{\partial Y^2}+M\frac{\partial \bar{H}_x}{\partial Y} \tag{2}$$

$$\frac{\partial \bar{H}_x}{\partial \tau}+U\frac{\partial \bar{H}_x}{\partial X}+V\frac{\partial \bar{H}_x}{\partial Y}=\bar{H}_x\frac{\partial U}{\partial X}+M\frac{\partial U}{\partial Y}+\frac{1}{P_m}\frac{\partial^2 \bar{H}_x}{\partial Y^2} \tag{3}$$

$$\frac{\partial \bar{T}}{\partial \tau}+U\frac{\partial \bar{T}}{\partial X}+V\frac{\partial \bar{T}}{\partial Y}=\frac{\partial^2 \bar{T}}{P_r\partial Y^2}+\frac{E_c}{P_m}\left(\frac{\partial \bar{H}_x}{\partial Y}\right)^2+E_c\left(\frac{\partial U}{\partial Y}\right)^2 \tag{4}$$

$$\frac{\partial \bar{C}}{\partial \tau}+U\frac{\partial \bar{C}}{\partial X}+V\frac{\partial \bar{C}}{\partial Y}=\frac{1}{S_c}\frac{\partial^2 \bar{C}}{\partial Y^2}+S_o\frac{\partial^2 \bar{T}}{\partial Y^2} \tag{5}$$

also the associated initial and boundary conditions are

$$\tau\le 0,\ U=0,\ V=0,\ \bar{H}_x=0,\ \bar{T}=0,\ \bar{C}=0\ \text{ everywhere} \tag{6}$$

$$\tau>0,\ U=0,\ V=0,\ \bar{H}_x=0,\ \bar{T}=0,\ \bar{C}=0\quad \text{at } X=0$$

$$U=1,\ V=0,\ \bar{H}_x=h=1(\text{say}),\ \bar{T}=1,\ \bar{C}=1\quad \text{at } Y=0 \tag{7}$$

$$U=0,\ V=0,\ \bar{H}_x=0,\ \bar{T}=0,\ \bar{C}=0\quad \text{as } Y\to\infty$$

3. SHEAR STRESS, CURRENT DENSITY, NUSSELT AND SHERWOOD NUMBER

From the velocity field, the effects of various parameters on the shear stress have been calculated. The local and average shear stress, $\tau_L=\mu\left(\frac{\partial U}{\partial Y}\right)_{Y=0}$ and $\tau_A=\mu\int\left(\frac{\partial U}{\partial Y}\right)_{Y=0}dX$ which are proportional to $\left(\frac{\partial U}{\partial Y}\right)_{Y=0}$ and $\int_0^{100}\left(\frac{\partial U}{\partial Y}\right)_{Y=0}dX$ respectively. From the induced magnetic field, the effects of various parameters on current density have been observed. The local and average current density, $J_L=\mu\left(-\frac{\partial \bar{H}_x}{\partial Y}\right)_{Y=0}$ and $J_A=\mu\int\left(-\frac{\partial \bar{H}_x}{\partial Y}\right)_{Y=0}dX$ which are proportional to $\left(-\frac{\partial \bar{H}_x}{\partial Y}\right)_{Y=0}$ and $\int_0^{100}\left(-\frac{\partial \bar{H}_x}{\partial Y}\right)_{Y=0}dX$ respectively. From the temperature field, the effects of various parameters on the Nusselt number have been investigated. The local and average Nusselt number, $N_{u_L}=\mu\left(-\frac{\partial \bar{T}}{\partial Y}\right)_{Y=0}$ and $N_{u_A}=\mu\int\left(-\frac{\partial \bar{T}}{\partial Y}\right)_{Y=0}dX$ which are proportional to $\left(-\frac{\partial \bar{T}}{\partial Y}\right)_{Y=0}$ and $\int_0^{100}\left(-\frac{\partial \bar{T}}{\partial Y}\right)_{Y=0}dX$ respectively. And from concentration field, the effects of various parameters on Sherwood number have been analyzed. The local and average Sherwood number, $S_{h_L}=\mu\left(-\frac{\partial \bar{C}}{\partial Y}\right)_{Y=0}$ and $S_{h_A}=\mu\int\left(-\frac{\partial \bar{C}}{\partial Y}\right)_{Y=0}dX$ which are proportional to $\left(-\frac{\partial \bar{C}}{\partial Y}\right)_{Y=0}$ and $\int_0^{100}\left(-\frac{\partial \bar{C}}{\partial Y}\right)_{Y=0}dX$.

4. NUMERICAL SOLUTIONS

In order to solve the non-dimensional system by the explicit finite difference method, it is required a set of finite difference equations. For this, a rectangular region of the flow field is chosen and the region is divided into a grid of lines parallel to X and Y axes, where X-axis is taken along the plate and Y-axis is normal to the plate. Here we consider that the plate of height $X_{\max}(=100)$ i.e. X varies from 0 to 100 and assumed $Y_{\max}(=25)$ as corresponding to $Y\to\infty$ i.e. Y varies from 0 to 25. There are $m(=125)$ and $n(=125)$ grid spacing in the X and Y directions respectively as shown in Fig 2. It is assumed that ΔX , ΔY are constant mesh sizes along X and Y directions respectively and taken as follows,

$\Delta X=0.8(0\le X\le 100)$ and $\Delta Y=0.2(0\le Y\le 25)$

with the smaller time-step,

$$\Delta\tau=0.005\,.$$

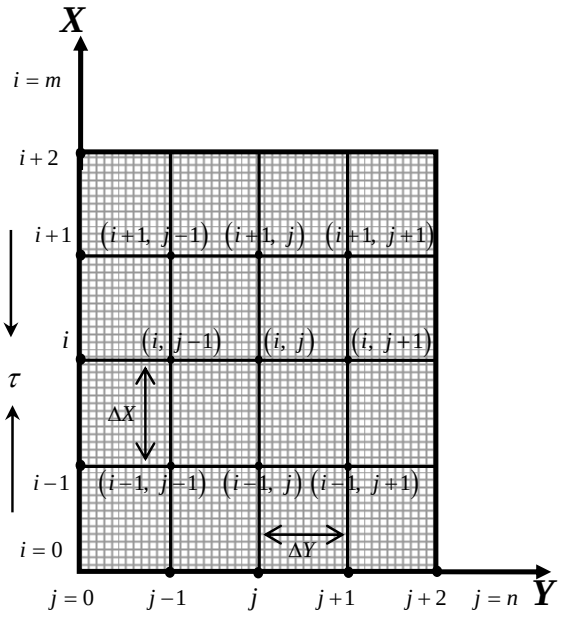

Fig 2. Finite difference space grid

Let U', V', $\bar{H}_x'$, $\bar{T}'$ and $\bar{C}'$ denote the values of U, V, $\bar{H}_x$, $\bar{T}$ and $\bar{C}$ at the end of a time-step respectively. Using the explicit finite difference approximation, we obtain the following appropriate set of finite difference equations;

$$\frac{U'_{i,j}-U'_{i-1,j}}{\Delta X}+\frac{V_{i,j}-V_{i,j-1}}{\Delta Y}=0 \tag{8}$$

$$\frac{U'_{i,j}-U_{i,j}}{\Delta\tau}+U_{i,j}\frac{U_{i,j}-U_{i-1,j}}{\Delta X}+V_{i,j}\frac{U_{i,j+1}-U_{i,j}}{\Delta Y}=G_r\bar{T}'_{i,j}$$
$$+G_m\bar{C}'_{i,j}+\frac{U_{i,j+1}-2U_{i,j}+U_{i,j-1}}{(\Delta Y)^2}+M\frac{\bar{H}_{x_{i,j+1}}-\bar{H}_{x_{i,j}}}{\Delta Y} \tag{9}$$

$$\frac{\bar{H}'_{x_{i,j}}-\bar{H}_{x_{i,j}}}{\Delta\tau}+U_{i,j}\frac{\bar{H}_{x_{i,j}}-\bar{H}_{x_{i-1,j}}}{\Delta X}+V_{i,j}\frac{\bar{H}_{x_{i,j+1}}-\bar{H}_{x_{i,j}}}{\Delta Y}=$$
$$\bar{H}_{x_{i,j}}\frac{U_{i,j}-U_{i-1,j}}{\Delta X}+M\frac{U_{i,j+1}-U_{i,j}}{\Delta Y}$$
$$+\frac{1}{P_m}\frac{\bar{H}_{x_{i,j+1}}-2\bar{H}_{x_{i,j}}+\bar{H}_{x_{i,j-1}}}{(\Delta Y)^2} \tag{10}$$

$$\frac{\bar{T}'_{i,j}-\bar{T}_{i,j}}{\Delta\tau}+U_{i,j}\frac{\bar{T}_{i,j}-\bar{T}_{i-1,j}}{\Delta X}+V_{i,j}\frac{\bar{T}_{i,j+1}-\bar{T}_{i,j}}{\Delta Y}=$$
$$\frac{1}{P_r}\frac{\bar{T}_{i,j+1}-2\bar{T}_{i,j}+\bar{T}_{i,j-1}}{(\Delta Y)^2}+\frac{E_c}{P_m}\left(\frac{\bar{H}_{x_{i,j+1}}-\bar{H}_{x_{i,j}}}{\Delta Y}\right)^2$$
$$+E_c\left(\frac{U_{i,j+1}-U_{i,j}}{\Delta Y}\right)^2 \tag{11}$$

$$\frac{\bar{C}'_{i,j}-\bar{C}_{i,j}}{\Delta\tau}+U_{i,j}\frac{\bar{C}_{i,j}-\bar{C}_{i-1,j}}{\Delta X}+V_{i,j}\frac{\bar{C}_{i,j+1}-\bar{C}_{i,j}}{\Delta Y}=$$
$$\frac{1}{S_c}\frac{\bar{C}_{i,j+1}-2\bar{C}_{i,j}+\bar{C}_{i,j-1}}{(\Delta Y)^2}+S_o\frac{\bar{T}_{i,j+1}-2\bar{T}_{i,j}+\bar{T}_{i,j-1}}{(\Delta Y)^2} \tag{12}$$

with initial and boundary conditions

$$U^0_{i,j}=0,\ V^0_{i,j}=0,\ \bar{H}^0_{x_{i,j}}=0,\ \bar{T}^0_{i,j}=0,\ \bar{C}^0_{i,j}=0 \tag{13}$$

$$U^n_{0,j}=0,\ V^n_{0,j}=0,\ \bar{H}^n_{x_{0,j}}=0,\ \bar{T}^0_{0,j}=0,\ \bar{C}^n_{0,j}=0$$
$$U^n_{i,0}=1,\ V^n_{i,0}=0,\ \bar{H}^n_{x_{i,0}}=1,\ \bar{T}^n_{i,0}=1,\ \bar{C}^n_{i,0}=1 \tag{14}$$
$$U^n_{i,L}=0,\ V^n_{i,L}=0,\ \bar{H}^n_{x_{i,L}}=0,\ \bar{T}^n_{i,L}=0,\ \bar{C}^n_{i,L}=0,\quad L\to\infty$$

Here the subscripts i and j designate the grid points with X and Y coordinates respectively and the superscript n represents a value of time, $\tau = n\Delta\tau$ where $n = 0, 1, 2, \ldots$. The stability conditions of the method are

$$U\frac{\Delta\tau}{\Delta X}+|V|\frac{\Delta\tau}{\Delta Y}+\frac{2}{P_r}\frac{\Delta\tau}{(\Delta Y)^2}\le 1,$$

$U\frac{\Delta\tau}{\Delta X}+|V|\frac{\Delta\tau}{\Delta Y}+\frac{2}{S_c}\frac{\Delta\tau}{(\Delta Y)^2}\le 1$ and convergence criteria of the method are $E_c \ll 1$, $P_r \ge 0.25$ and $S_c \ge 0.25$.

5. RESULTS AND DISCUSSION

To observe the physical situation of the problem, we have illustrated the steady-state local and average shear stress, current density, Nusselt number and Sherwood number versus X and τ respectively in Figs 3-20. The effect of M, S_o, E_c, G_r, P_r and S_c on shear stress are shown in Figs 3-8. We see that both steady-state local and average shear stress increase with the rise of S_o, E_c or G_r while decrease with the increase of M, P_r or S_c. It is concluded that the shear stress is greater for air and helium than water and carbondioxide respectively.

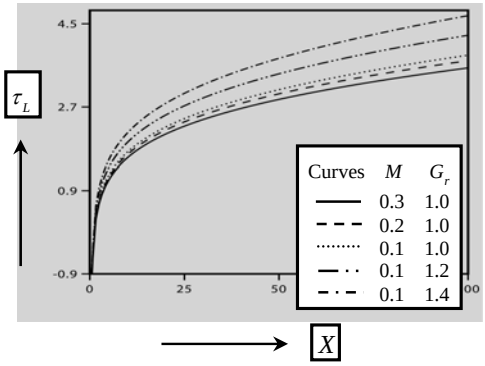

Fig 3. Steady-state local shear stress for $G_m = 0.4$, $P_r = 0.71$, $S_c = 0.6$, $S_o = 1$, $P_m = 1$ & $E_c = 0.01$.

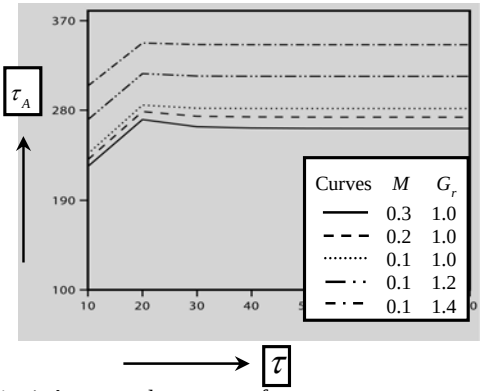

Fig 4. Average shear stress for $G_m = 0.4$, $P_r = 0.71$,

$S_c = 0.6,\ S_o = 1,\ P_m = 1$ & $E_c = 0.01$.

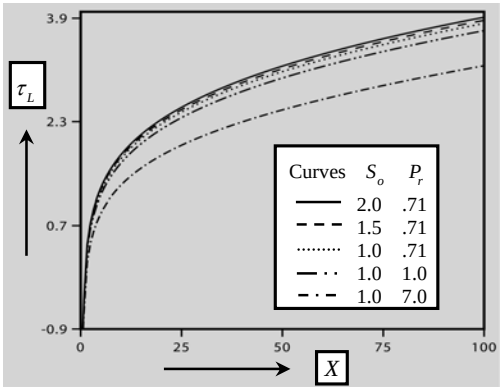

Fig 5. Steady-state local shear stress for $G_r = 1$, $G_m = 0.4$, $M = 0.1$, $S_c = 0.6$, $P_m = 1$ & $E_c = 0.01$.

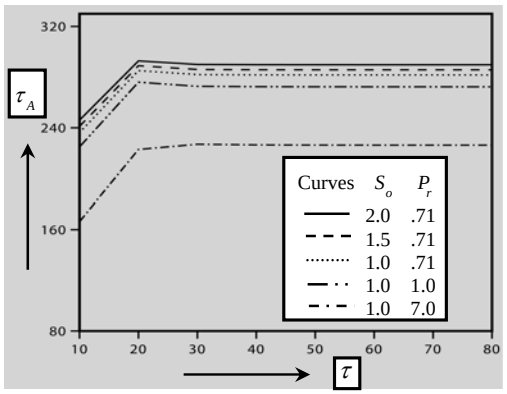

Fig 6. Average shear stress for $G_r = 1$, $G_m = 0.4$, $M = 0.1$, $S_c = 0.6$, $P_m = 1$ & $E_c = 0.01$.

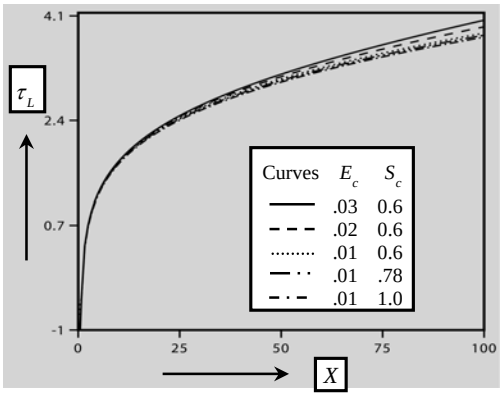

Fig 7. Steady-state local shear stress for $G_r = 1$, $G_m = 0.4$, $M = 0.1$, $P_r = 0.71$, $S_o = 1$ & $P_m = 1$.

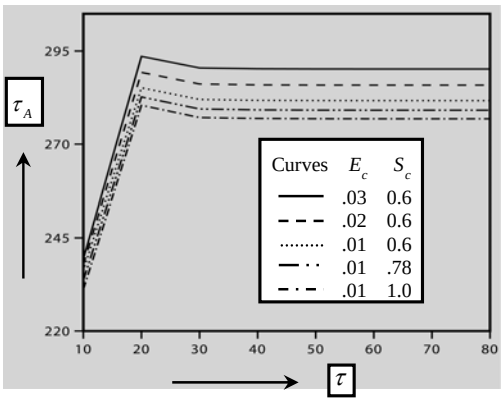

Fig 8. Average shear stress for $G_r = 1$, $G_m = 0.4$, $M = 0.1$, $P_r = 0.71$, $S_o = 1$ & $P_m = 1$.

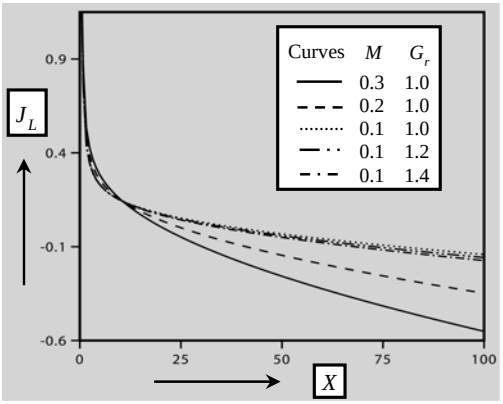

Fig 9. Steady-state local current density for $G_m = 0.4$, $P_r = 0.71$, $S_c = 0.6$, $S_o = 1$, $P_m = 1$ & $E_c = 0.01$.

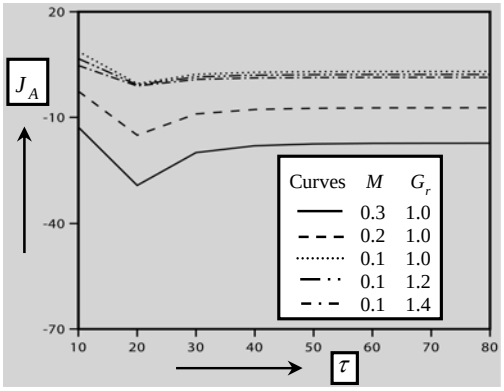

Fig 10. Average current density for $G_m = 0.4$, $P_r = 0.71$, $S_c = 0.6$, $S_o = 1$, $P_m = 1$ & $E_c = 0.01$.

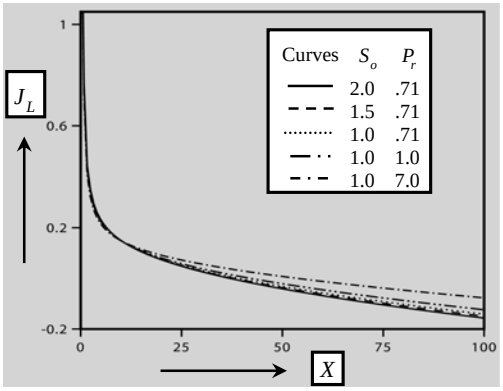

Fig 11. Steady-state local current density for $G_r = 1$, $G_m = 0.4$, $M = 0.1$, $S_c = 0.6$, $P_m = 1$ & $E_c = 0.01$.

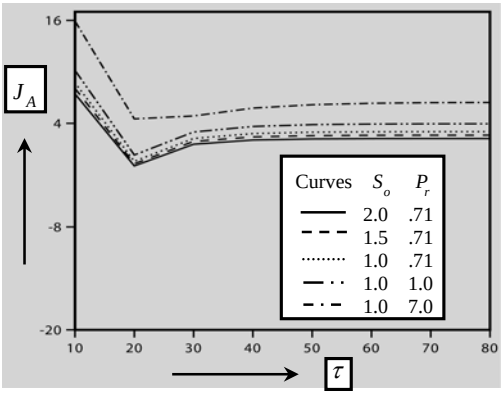

Fig 12. Average current density for $G_r = 1$, $G_m = 0.4$, $M = 0.1$, $S_c = 0.6$, $P_m = 1$ & $E_c = 0.01$.

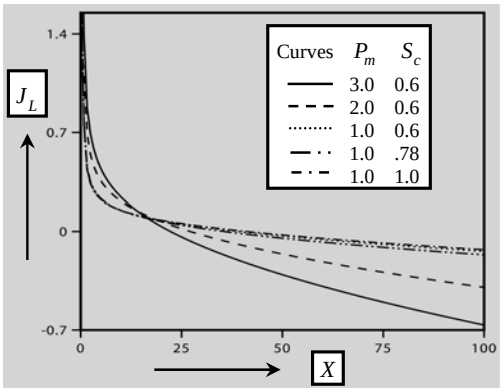

Fig 13. Steady-state local current density for $G_r = 1$, $G_m = 0.4$, $M = 0.1$, $P_r = 0.71$, $S_o = 1$ & $E_c = 0.01$.

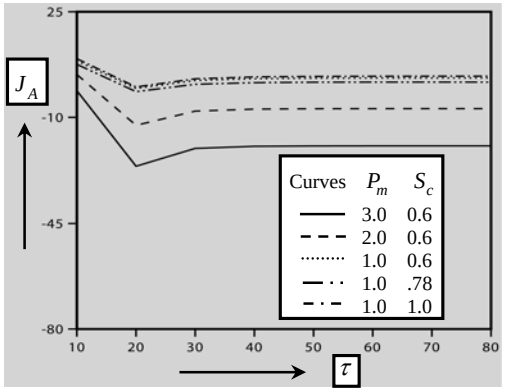

Fig 14. Average current density for $G_r = 1$, $G_m = 0.4$, $M = 0.1$, $P_r = 0.71$, $S_o = 1$ & $E_c = 0.01$.

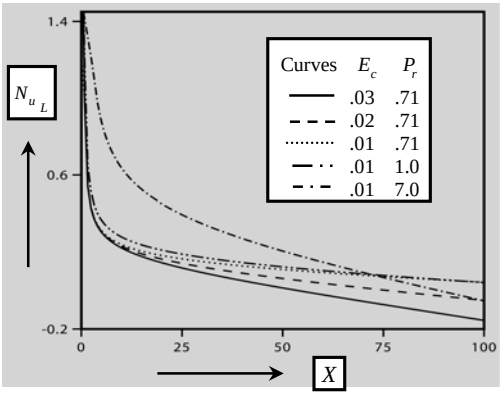

Fig 15. Steady-state local Nusselt number for $G_r = 1$, $G_m = 0.4$, $M = 0.1$, $S_c = 0.6$, $P_m = 1$ & $S_o = 1$.

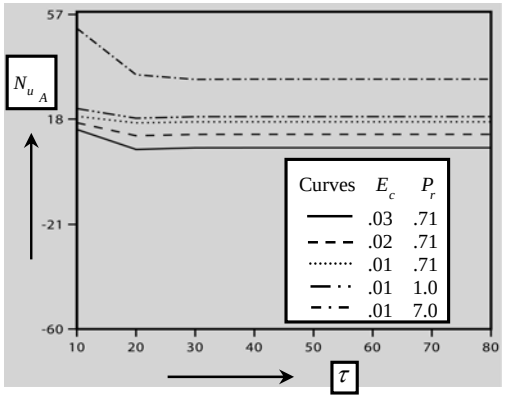

Fig 16. Average Nusselt number for $G_r = 1$, $G_m = 0.4$, $M = 0.1$, $S_c = 0.6$, $P_m = 1$ & $S_o = 1$.

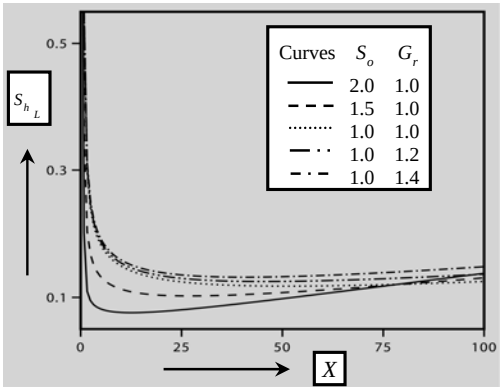

Fig 17. Steady-state local Sherwood number for $P_m = 1,\ G_m = .4,\ P_r = .71,\ S_c = .6,\ M = .1$ & $E_c = .01$.

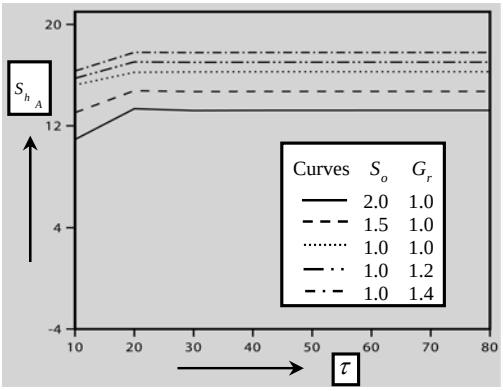

Fig 18. Average Sherwood number for $G_m = 0.4,\ P_r = 0.71,\ S_c = 0.6,\ M = 0.1,\ P_m = 1$ & $E_c = 0.01$.

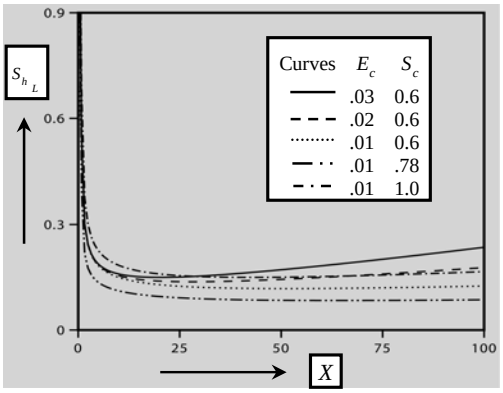

Fig 19. Steady-state local Sherwood number for $G_r = 1,\ G_m = 0.4,\ M = 0.1,\ P_r = 0.71,\ S_o = 1$ & $P_m = 1$.

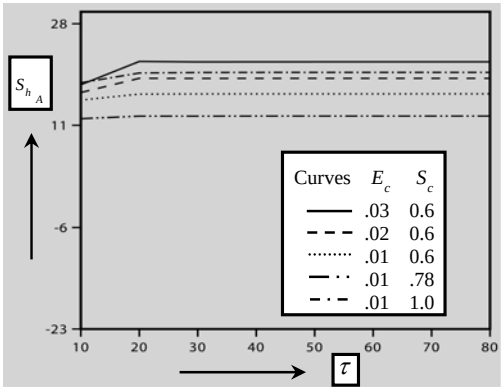

Fig 20. Average Sherwood number for $G_r = 1,\ G_m = 0.4,\ M = 0.1,\ P_r = 0.71,\ S_o = 1$ & $P_m = 1$.

The profiles of steady-state local and average current density for different values of M, S_o, P_r, G_r, P_m and S_c are presented in Figs 9-14. We observe from these figures, both the steady-state local and average current density increase in case of strong P_r or S_c while decrease with the increase of M, S_o, G_r or P_m. It is noted that the current density is more for water and carbondioxide than air and helium respectively.

The curves of steady-state local and average Nusselt number are displayed in Figs 15-16 for different values of E_c and P_r. It is found that both local and average Nusselt number rise with the increase of Prandtl number but fall with the increase of E_c. It is declared that the Nusselt number is greater for water than air.

The distributions of steady-state local and average Sherwood number have been shown in Figs. 17-20 for the different values of S_o, E_c, G_r and S_c. Both the local and average Sherwood number increase in case of strong E_c, G_r or S_c while decrease with the rise of S_o. It is concluded that the Sherwood number is more for carbondioxide than helium.

Finally, a comparison of our results is made with both analytical solutions for the natural convective problem at a heated vertical plate given by Ostrach[8] and numerical solutions given by Allam and Sattar[6] with no magnetic and rotation effects in their problem. If the viscous dissipation and joule heating terms are neglected in energy equation as well as no magnetic effect, no uniform velocity U_0 are assumed in our problem, it reduces to the problem considered by Ostrach[8]. Hence the comparison of the present results with analytical and numerical results are presented in Table 1 for steady-state $\tau = 80$. The accuracy of the present results may be good in case of all the flow variables.

Table 1. Comparison of the present steady-state results

Y	0			5.0			10.0			15.0		
Analytical results due to **Ostrach** [8] 39×39 grid, $\Delta\tau = 0.1$	U	V	$\bar{T}$	U	V	$\bar{T}$	U	V	$\bar{T}$	U	V	$\bar{T}$
	0	0	1	5.3	-.1	.5	2.8	-.3	.1	.9	-.3	.04
Numerical results due to **Alam** & **Sattar**[6] 10×10 grid, $\Delta\tau = 0.5$	0	0	1	5.0	-.1	.5	2.9	-.3	.2	1.1	-.4	.05
	Truncation error			**. 3**	**0**	**0**	**-.1**	**0**	**-.1**	**-.2**	**.1**	
Present results 125×125 grid, $\Delta\tau = 0.005$	0	0	1	5.4	-.1	.5	2.8	-.2	.1	.9	-.3	.04
	Truncation error			**-.1**	**0**	**0**	**0**	**-.1**	**0**	**0**	**0**	

6. REFERENCES

1. Raptis, A. and Singh, A. K., 1983, "MHD Free Convection Flow Past an Accelerated Vertical Plate", Int. Communications in Heat and Mass Transfer, 10:313.
2. Singh, A. K., Singh, Aj. K. and Singh, N. P., 2003, "Hydromagnetic Heat and Mass Transfer in a Flow of a Viscous Incompressible Fluid Past an Infinite Vertical Porous Plate under Oscillatory Suction Velocity Normal to the Plate", Indian Journal of Pure and Applied Mathematics, 34:429.
3. Sami, A. and Al-Sanea, 2004, "Mixed Convection Heat Transfer along a Continuously Moving Heated Vertical Plate with Suction or Injection", Int. J. Heat Mass Transfer, 47:1445.
4. Chamkha, A. J., 2004, "Unsteady MHD Convective Heat and Mass Transfer Past a Semi-infinite Vertical Permeable Moving Plate with Heat Absorption", Int. J. Engg. Sci., 42:217.
5. Eckert, E. R. G. and Drake, R.M., 1972, "Analysis of Heat and Mass Transfer", McGraw-Hill Book Co., New York.
6. Alam, M. M. and Sattar, M. A., 1999, "Transient MHD Heat and Mass Transfer Flow with Thermal Diffusion in a Rotating System", J. of Energy, Heat and Mass Transfer, 21:09.
7. Alam, M. S., Rahman, M. M. and Samad, M. A., 2006, "Numerical Study of the Combined Free-forced Convection and Mass Transfer Flow Past a Vertical Porous Medium with Heat Generation and Thermal Diffusion", Nonlinear analysis: Modeling and Control, 11(4):331.
8. Ostrach, S., 1953, "An Analysis of Laminer Free-convection Flow and Heat Transfer about a Flate Plate Parallel to the Direction of the Generation Body Force", Natl. Advisory Comm. Aeronautical Technology Report, 1111.

7. NOMENCLATURE

Symbol	Meaning	Unit
x, y	Cartesian coordinates	
u, v	Velocity components	(ms^{-1})
υ	Kinematic viscosity	(m^2s^{-1})
ρ	Density of fluid	(kgm^{-3})
μ_e	Magnetic permeability	
τ	Dimensionless time	
X, Y	Dimensionless cartesian coordinates	
U, V	Dimensionless velocity components	
$\bar{H}_x$	Dimensionless induced magnetic field vector	
$\bar{T}$	Dimensionless temperature	
$\bar{C}$	Dimensionless concentration	
G_r	Grashof number	
G_m	Modified Grashof number	
M	Magnetic Force number	
P_m	Magnetic diffusivity number	
P_r	Prandtl number	
E_c	Eckert number	
S_c	Schmidt Number	
S_o	Soret Number	
μ	Coefficient of viscosity	

8. MAILING ADDRESS

Md. Mohidul Haque
Mathematics Discipline,
Khulna University, Khulna, Bangladesh